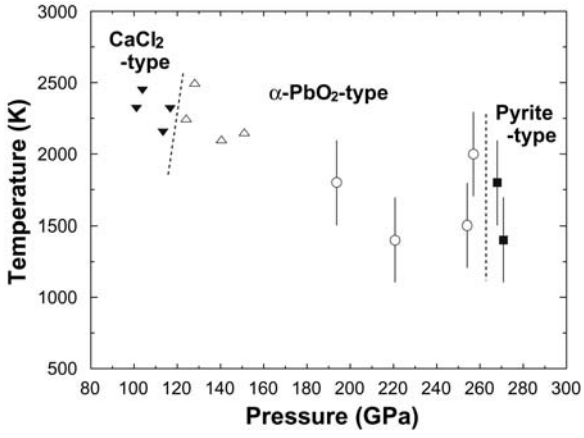

Fig. 3. Phase diagram of SiO_2. Open circles and solid squares indicate the stabilities of the α-PbO_2-type and pyrite-type phases, respectively. Solid reversed triangles and open triangles show previous experimental data (*7*) on the stabilities of the $CaCl_2$-type and α-PbO_2-type phases, respectively. The dotted lines show the tentative phase boundary.

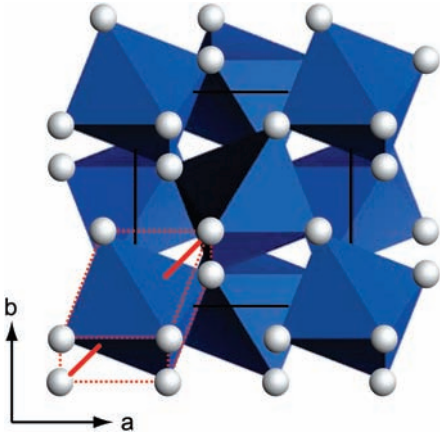

Fig. 4. Crystal structure of pyrite-type silica. Coordination polyhedra of O atoms around Si atoms are shown as octahedra. O atoms are illustrated as balls. The black line indicates the unit cell, and bold red lines show the second nearest bonds. 6+2 coordination polyhedra are illustrated by dotted red lines.

distance in pyrite-type silica is 2.063(6) Å (Table 1), consistent with theoretical calculations set at 0 K (*11*, *13*), which is much longer than the typical distance of single covalent O–O bonds (~1.5 Å). These experimental data support the arguments that there are no O–O covalent bonds in pyrite-type silica (*13*).

Silica is the most abundant oxide component in the Earth's crust and mantle, but the pressure required for the pyrite type is greater than that found in the Earth's mantle. Nevertheless, it is also one of the most important oxide components in other planets of our solar system. Theoretical modelling of the interiors of ice giant planets suggests that both Uranus and Neptune may have a rocky core at pressures about 800 GPa and below (*21*), and therefore the pyrite-type silica might be an important constituent of these planets. Moreover, silicates are significant oxide components in extrasolar systems (*22*). During the formation of terrestrial planets, pressures may exceed 260 GPa and thus include the pyrite-type silica phase.

References and Notes

1. R. J. Hemley, C. T. Prewitt, K. J. Kingma, in *Silica*, P. J. Heaney, C. T. Prewitt, G. V. Gibbs, Eds. (Mineralogical Society of America, Washington, DC, 1994), pp. 41–84.
2. Y. Tsuchida, T. Yagi, *Nature* **340**, 217 (1989).
3. K. J. Kingma, R. E. Cohen, R. J. Hemley, H. K. Mao, *Nature* **374**, 243 (1995).
4. D. Andrault, G. Fiquet, F. Guyot, M. Hanfland, *Science* **282**, 720 (1998).
5. S. Ono, K. Hirose, M. Murakami, M. Isshiki, *Earth Planet. Sci. Lett.* **197**, 187 (2002).
6. L. S. Dubrovinsky *et al.*, *Nature* **388**, 362 (1997).
7. M. Murakami, K. Hirose, S. Ono, Y. Ohishi, *Geophys. Res. Lett.* **30**, 1207, doi:10.1029/2002GL016722 (2003).
8. J. Haines, J. M. Léger, F. Gorelli, M. Hanfland, *Phys. Rev. Lett.* **87**, 155503 (2001).
9. L. S. Dubrovinsky *et al.*, *Phys. Earth Planet. Inter.* **143–144**, 231 (2004).
10. K. T. Park, K. Terakura, Y. Matsui, *Nature* **336**, 670 (1988).
11. B. B. Karki, M. C. Warren, L. Stixrude, G. J. Ackland, J. Crain, *Phys. Rev. B* **55**, 3465 (1997).
12. D. M. Teter, R. J. Hemley, G. Kresse, J. Hafner, *Phys. Rev. Lett.* **80**, 2145 (1998).
13. A. R. Oganov, M. J. Gillan, G. D. Price, *Phys. Rev. B* **71**, 064104 (2005).
14. Angle-dispersive XRD spectra were obtained on an imaging plate (Rigaku R-AXIS IV) and x-ray charge-coupled device (Bruker APEX) at BL10XU of SPring-8. The incident x-rays were monochromatized to a wavelength of 0.41045 or 0.41296 Å. The x-ray beam was collimated to 20 μm in diameter. Two-dimensional diffraction images were integrated as a function of 2-theta in order to give conventional one-dimensional diffraction profiles (*23*).
15. G. Shen, H. K. Mao, R. J. Hemley, *Proceedings of the 3rd NIRIM International Symposium on Advanced Materials* (National Institute for Research in Inorganic Materials, Tsukuba, Japan, 1996), pp. 149–152.
16. T. Watanuki, O. Shimomura, T. Yagi, T. Kondo, M. Isshiki, *Rev. Sci. Instrum.* **72**, 1289 (2001).
17. N. C. Holmes, J. A. Moriarty, G. R. Gathers, W. J. Nellis, *J. Appl. Phys.* **66**, 2962 (1989).
18. F. Izumi, T. Ikeda, *Mater. Sci. Forum* **198**, 321 (2000).
19. J. Haines, J. M. Léger, O. Schulte, *Science* **271**, 629 (1996).
20. S. Ono, T. Tsuchiya, K. Hirose, Y. Ohishi, *Phys. Rev. B* **68**, 014103 (2003).
21. T. Guillot, *Science* **286**, 72 (1999).
22. J. B. Pollack *et al.*, *Astrophys. J.* **421**, 615 (1994).
23. A. P. Hammersley, European Synchrotron Radiation Facility internal report no. ESRF97HA02T (European Synchrotron Radiation Facility, Grenoble, France, 1997).

24. We thank K. Kawamura, T. Tsuchiya, H. Genda, M. Ikoma, Y. Tatsumi, T. Suzuki, and S. Ono for discussions. In situ XRD measurements were conducted at SPring-8 (proposal no. 2004B4013-LD2-np and 2005A5013-LD2-np). Y.K. was supported by the Japan Society for the Promotion of Science Research Fellowships for Young Scientists.

16 May 2005; accepted 29 June 2005
10.1126/science.1114879

Ice Sheet and Solid Earth Influences on Far-Field Sea-Level Histories

Sophie E. Bassett,[1] Glenn A. Milne,[1]* Jerry X. Mitrovica,[2] Peter U. Clark[3]

Previous predictions of sea-level change subsequent to the last glacial maximum show significant, systematic discrepancies between observations at Tahiti, Huon Peninsula, and Sunda Shelf during Lateglacial time (~14,000 to 9000 calibrated years before the present). We demonstrate that a model of glacial isostatic adjustment characterized by both a high-viscosity lower mantle (4×10^{22} Pa s) and a large contribution from the Antarctic ice sheet to meltwater pulse IA (~15-meters eustatic equivalent) resolves these discrepancies. This result supports arguments that an early and rapid Antarctic deglaciation contributed to a sequence of climatic events that ended the most recent glacial period of the current ice age.

The evolution of high-latitude global ice volumes, as inferred from observations of far-field sea-level change, serves as a fundamental constraint on ice-age climate models (*1*). In this regard, data from Barbados (*2*, *3*), the Sunda Shelf (*4*), Tahiti (*5*), Huon Peninsula (*6*, *7*) and the Bonaparte Gulf (*8*) (Fig. 1) record a spatially and temporally variable sea-level history that samples ice sheet fluctuations through the complex, modulating influence of glacial isostatic adjustment (GIA) (*9*–*11*). Efforts to fit these histories with global ice reconstructions and

[1]Department of Earth Sciences, University of Durham, Durham DH1 3LE, UK. [2]Department of Physics, University of Toronto, Toronto, Ontario M5S 1A7, Canada. [3]Department of Geosciences, Oregon State University, Corvallis, OR 97331, USA.

*To whom correspondence should be addressed. E-mail: g.a.milne@durham.ac.uk

numerical models of GIA-induced sea-level change have been characterized by enigmatic and highly contentious misfits (*11*–*14*) at several key sites, particularly during the Lateglacial period [~14 to 9 calibrated kiloyears before present (cal kyr BP)] (*11*). Here, we investigate the origin of these Lateglacial misfits and explore whether they might be reconciled through a revision of widely adopted ice histories or Earth model parameters.

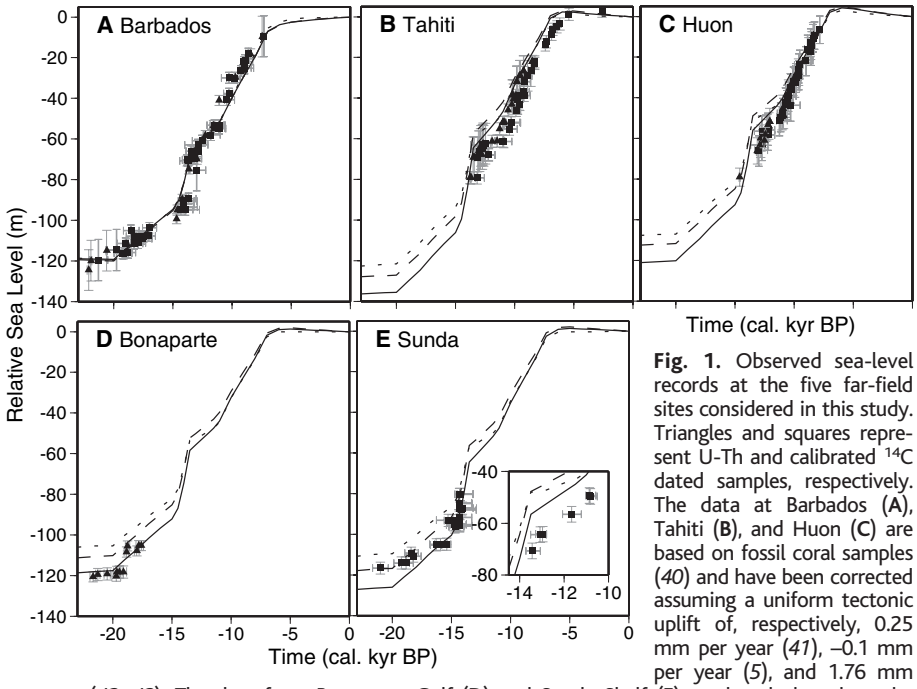

Fig. 1. Observed sea-level records at the five far-field sites considered in this study. Triangles and squares represent U-Th and calibrated ^{14}C dated samples, respectively. The data at Barbados (**A**), Tahiti (**B**), and Huon (**C**) are based on fossil coral samples (*40*) and have been corrected assuming a uniform tectonic uplift of, respectively, 0.25 mm per year (*41*), –0.1 mm per year (*5*), and 1.76 mm per year (*42*, *43*). The data from Bonaparte Gulf (**D**) and Sunda Shelf (**E**) are largely based on the analysis of organic material found in sediment cores. No tectonic correction has been applied to these data. Sea-level markers at Sunda Shelf are collected from two regions displaced by as much as ~800 km (*4*), and numerical predictions show significant differential trends across this zone (*9*). Accordingly, data (and predictions) in (E) are separated into two subsets, one from the southern zone of collection (main figure) and the other from the northern zone (inset). The lines on each panel are site-dependent numerical predictions of post-LGM sea-level change and are based on ice history that includes a dominant North American source for the mwp-IA event. The predictions are distinguished on the basis of the lower mantle viscosity of the adopted Earth model: dotted line, 2×10^{21} Pa s; dashed line, 10^{22} Pa s; and solid line, 4×10^{22} Pa s.

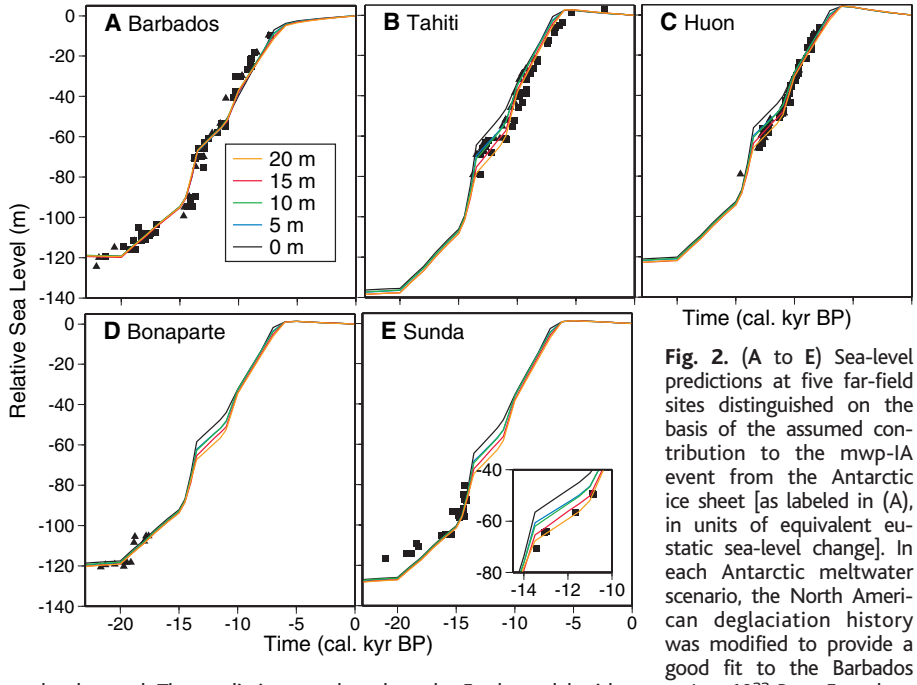

Fig. 2. (**A** to **E**) Sea-level predictions at five far-field sites distinguished on the basis of the assumed contribution to the mwp-IA event from the Antarctic ice sheet [as labeled in (A), in units of equivalent eustatic sea-level change]. In each Antarctic meltwater scenario, the North American deglaciation history was modified to provide a good fit to the Barbados sea-level record. The predictions are based on the Earth model with $\nu_{LM} = 4 \times 10^{22}$ Pa s. Error bars have been omitted to improve clarity. The inset of panel (E) compares predictions with the observations derived from the more northerly subset of the cores.

To illustrate the nature of the misfits, we superimpose GIA predictions onto the observed sea-level records in Fig. 1 that were generated by spherically symmetric, self-gravitating, and viscoelastic Earth models with density and elastic structure taken from seismic constraints (*15*). The Earth models are characterized by a 100-km-thick elastic lithosphere and a sublithospheric upper mantle viscosity of 5×10^{20} Pa s; the predictions are distinguished on the basis of the adopted lower mantle viscosity (below a depth of 670 km). For each choice of lower mantle viscosity (ν_{LM}), the adopted ice model was modified (*16*) from the global ICE-3G deglaciation history (*17*) to fit the Barbados sea-level record. This modification involved the inclusion of a dominant North American source (*18*) for meltwater pulse IA (mwp-IA), as in the more recent ICE-4G and ICE-5G deglaciation models (*19*, *20*); the mwp-IA event, first identified in the Barbados record (*2*, *3*), resulted in a eustatic sea level rise of ~20 to 25 m between 14.5 and 13.5 cal kyr BP. The sea-level predictions are based on an algorithm (*21*) that includes an accurate treatment (*22*–*24*) of time-evolving continental shorelines and feedback from Earth-rotation perturbations.

Our focus is the ~5-kyr period subsequent to the mwp-IA event (the Lateglacial period). The dotted line in Fig. 1 was generated by an ice and Earth model ($\nu_{LM} = 2 \times 10^{21}$ Pa s) broadly similar to several earlier GIA studies (*11*, *19*). This ice history and Earth model combination, tuned to closely match the Barbados record, yields a poor fit to the Lateglacial sea-level histories in the Huon Peninsula, Tahiti, and Sunda Shelf (Fig. 1E, inset); in these cases, the predictions are too shallow by ~20 m. A similar misfit between an earlier GIA prediction (*19*) and data at Huon Peninsula was noted by Edwards (*12*), who questioned the accuracy of the GIA model; Peltier (*13*) suggested, in contrast, that the steady tectonic correction of 1.9 mm per year applied to the raw data (*6*, *12*) was suspect. This argument has been reiterated in more recent work (*11*, *14*), where it is cited to explain "extremely large" (~30-m) discrepancies at both Huon and Tahiti (*11*). The possibility has also been raised that the misfits reflect a change in the living depth of coral assemblages from Lateglacial to early Holocene times (*11*, *25*).

A lower mantle viscosity of 2×10^{21} Pa s is not compatible with a number of recent inferences based on data associated with GIA and/or mantle convection (*26*–*28*). Lambeck *et al.* (*9*) recently explored fits between GIA

predictions and far-field relative sea-level data before and after the last glacial maximum (LGM) and concluded that discrepancies over this broad time window are reduced as ν_{LM} is increased to values of $\sim 3 \times 10^{22}$ Pa s (*29*). The remaining lines in Fig. 1, which sample ν_{LM} values of 10^{22} Pa s (dashed line) and 4×10^{22} Pa s (solid line), support this conclusion. The discrepancies during the Lateglacial period are ~50% less for the latter model compared with those of the original case of $\nu_{LM} = 2 \times 10^{21}$ Pa s. Furthermore, increasing the lower mantle viscosity of the Earth model to 4×10^{22} Pa s improves the fits to the oldest Bonaparte Gulf data (*9*). However, this model overpredicts the LGM lowstand at Sunda Shelf by ~10 m. The origin of this misfit is unclear, though it has been suggested that the bulk sediment analysis used to date the oldest sections of the core at this site may have biased the ages upward by as much as several thousand years (*9*).

Increasing the lower mantle viscosity above 4×10^{22} Pa s produces no further improvement in the fit to the post-LGM sea-level records. This is clear from fig. S1A (dashed line), which tracks the χ^2 misfit of this sequence of post-LGM predictions as a function of ν_{LM}.

The large residual misfit evident in Fig. 1 at Tahiti, Huon, and Sunda Shelf (Fig. 1E, inset) during the Lateglacial period appears to be exacerbated by the inclusion of the mwp-IA event into the adopted ice history in an effort to reconcile the Barbados record (*11*). This suggests that the discrepancies might be associated with an error in the adopted ice history, namely the distribution of the total meltwater flux among the various ice complexes during the massive mwp-IA event. An obvious target of investigation is therefore the primary source region for this event, which immediately precedes the Lateglacial time window. Clark *et al*. (*30*) argued that the relative size of the observed sea-level jump across mwp-IA (i.e., across 14.5 to 13.5 cal kyr BP) at Barbados and Sunda Shelf precludes a sole North American source for the event. Their analysis highlighted several possible mwp-IA scenarios (*31*), including a potentially large Antarctic contribution to the event. This specific suggestion is supported by climate models that indicate that a freshwater flux into the Southern Ocean provides a trigger for the Bølling-Allerød warm interval (*32*) and by South Atlantic records of contemporaneous (to mwp-IA) ice-rafted debris originating from the Antarctic ice sheet (*33*).

In Fig. 2, we show a suite of predictions in which the contribution of the Antarctic ice sheet to mwp-IA is varied from 0 m (as in Fig. 1) to 20 m of equivalent eustatic sea-level rise for the Earth model in which $\nu_{LM} = 4 \times 10^{22}$ Pa s. As the magnitude of the mass flux from the Antarctic ice sheet is increased, the contribution from the North American ice complex is suitably decreased to maintain a good fit to the Barbados record. The discrepancies between predictions and the Lateglacial sea-level trends recorded at Tahiti, Huon Peninsula, and Sunda Shelf (Fig. 1E, inset) are significantly reduced when an Antarctic component to mwp-IA is introduced.

Figure S1B shows the variation in the χ^2 misfit as this balance in meltwater source is altered. Because the variation in the predictions is most pronounced over the Lateglacial period (~14 to 9 cal kyr BP; Fig. 2), the misfit in fig. S1B is computed over this time window. The statistical tests directly reflect the results shown in Fig. 2: The model fit is improved to greater than 99% confidence, compared with the dominant North American scenario, when a substantial portion (~5 m or more) of mwp-IA is source from Antarctica. The quality of fit for the 5- and 10-m Antarctic source models is similar. A further significant improvement in fit was obtained when the magnitude was increased to 15 or 20 m; the data from Sunda Shelf, in particular, benefit from this increase in the Antarctic contribution (Fig. 2E, inset). We adopted the 15-m Antarctic scenario, which includes ~8 m from northern hemisphere sources (~6 m from North America), as the optimal model in consideration of recent independent constraints on the volume of the LGM Antarctic ice sheet (*34*, *35*).

The improvement in the fit is due to a number of factors. The change in the direct grav-

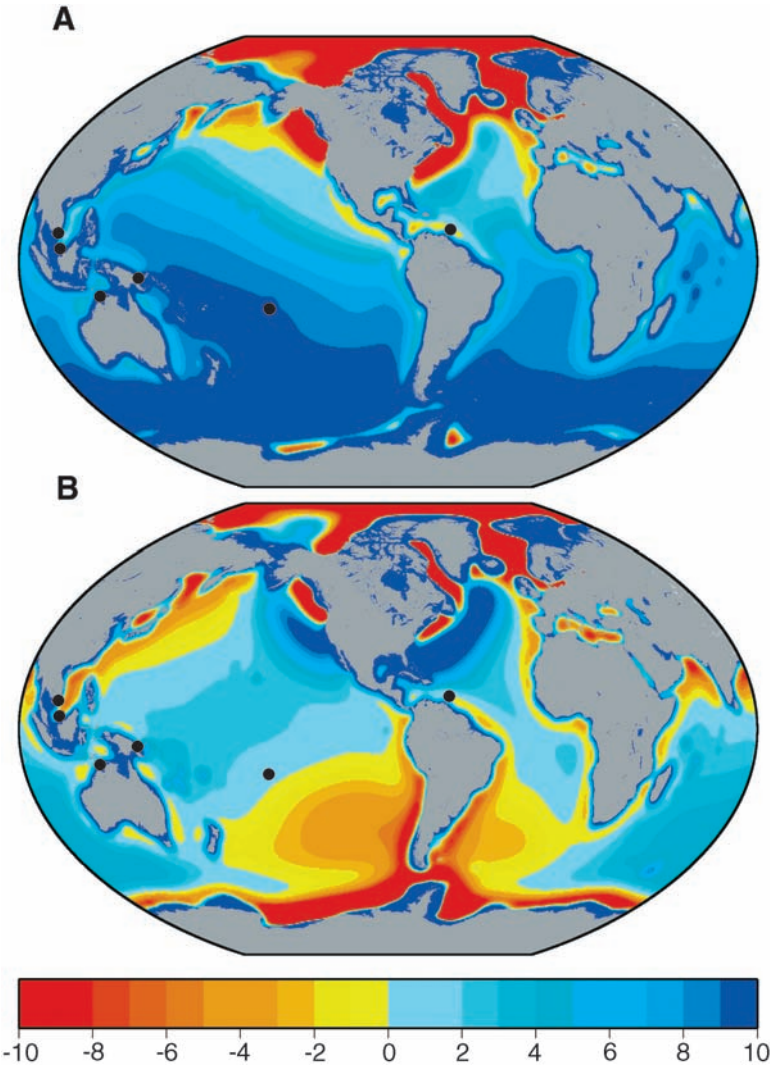

Fig. 3. Predicted sea-level change, in meters, over the past 13 cal kyr relative to the predicted change at Barbados (i.e., predictions of the raw sea-level change across this time interval are shifted by the specific prediction at Barbados, and thus the Barbados prediction falls on the zero contour in each panel). (**A**) The scenario in which North American ice is the sole source for the mwp-IA event (as in the predictions of Fig. 1; $\nu_{LM} = 4 \times 10^{22}$ Pa s). (**B**) The scenario assuming that the Antarctic ice sheet contributes an equivalent eustatic sea-level rise of 15 m to the event (as in the predictions shown by red lines in Fig. 2).

itational effect of the surface mass load as the Antarctic proportion of the mwp-IA source is increased reduces the magnitude of the sea-level rise across the event at the three southern sites (*30*, *36*). In addition, the viscoelastic response of the planet plays an important role in the isostatic adjustment following mwp-IA. Maps of the predicted sea-level change over the past 13 cal kyr (i.e., relative sea-level change since Lateglacial time) for the scenarios in which the Antarctic ice complex contributes either 0 or 15 m to mwp-IA (Fig. 3) indicate a significant change in the geometry of the associated GIA effects. Each map is plotted relative to the prediction at Barbados. The observed relative sea level of markers of age ~13 cal kyr BP at Barbados, Tahiti, Huon Peninsula, and Sunda Shelf are all at a depth of ~60 m (Figs. 1 and 2). In the scenario where Antarctic mass flux dominates the mwp-IA event (Fig. 3B), the predicted zero contour passes close to each of these sites and thus the 13 cal kyr BP relative sea-level markers are fit by this scenario. In contrast, the dominant North American source for mwp-IA yields significantly more discrepant predictions at these four sites (Fig. 3A).

We considered two additional mwp-IA source scenarios: a global distribution of sources based on the "All–ICE-3G" scenario described in (*30*) and a northern hemisphere source distribution based on the "North–ICE-3G" scenario described in (*30*) (fig. S2). The northern hemisphere model produces a fit very similar to that generated for the case of a dominant North American source, giving a relatively high χ^2 value of 15.7 over the Lateglacial period (compare this with fig. S1B). In comparison, the global source model provides an improved fit (χ^2 of 8.5) but there remain systematic discrepancies at Huon Peninsula and Sunda Shelf that are resolved when a larger (15-m) Antarctic contribution is adopted.

We conclude that the Lateglacial far-field sea-level record is a powerful constraint for testing a range of plausible mwp-IA source scenarios and that a substantial Antarctic contribution is a robust requirement of the data.

Inspection of the Barbados sea-level record has led to suggestions of a meltwater event (mwp-IB) with onset at 11.5 cal kyr BP; however, the existence of the event has remained controversial (*5*, *37*). To explore this issue, we altered our optimal ice model (15-m Antarctic scenario) to consider two models that include the mwp-IB event (fig. S3). The revised models produce a moderately improved fit to the early Holocene sea-level record at Barbados, but they introduce large discrepancies in the records at Tahiti and the Huon Peninsula over the same time period. Thus, our analysis does not support the existence of the mwp-IB event.

We show that long-debated discrepancies between predictions and observations of Lateglacial sea levels at Tahiti, Huon Peninsula, and Sunda Shelf can be reconciled by adopting both a relatively high lower mantle viscosity and a large (~15-m eustatic) contribution to mwp-IA from the Antarctic ice sheet. This conclusion is contrary to previous suggestions that the discrepancy is due to uncertainties in the habitation depth of coral species or errors in the tectonic corrections applied to the raw sea-level markers (*11*, *13*). Our results focus further attention on the Antarctic ice sheet as a key trigger for climatic events that led the Earth system out of the previous glacial period (*32*), and they add to our growing understanding (*9*, *10*) of the complex space-time mapping between ice sheet ablation and global sea-level change.

References and Notes

1. K. Lambeck, T. M. Esat, E.-K. Potter, *Nature* **419**, 199 (2002).
2. R. G. Fairbanks, *Nature* **342**, 637 (1989).
3. E. Bard, B. Hamelin, R. G. Fairbanks, A. Zindler, *Nature* **345**, 405 (1990).
4. T. Hanebuth, K. Stattegger, P. M. Grootes, *Science* **288**, 1033 (2000).
5. E. Bard *et al.*, *Nature* **382**, 241 (1996).
6. J. Chappell, H. Polach, *Nature* **349**, 147 (1991).
7. K. B. Cutler *et al.*, *Earth Planet. Sci. Lett.* **206**, 253 (2003).
8. Y. Yokoyama, K. Lambeck, P. De Dekker, P. Johnston, L. K. Fifield, *Nature* **406**, 713 (2000).
9. K. Lambeck, Y. Yokoyama, T. Purcell, *Quat. Sci. Rev.* **21**, 343 (2002).
10. G. A. Milne, J. X. Mitrovica, D. P. Schrag, *Quat. Sci. Rev.* **21**, 361 (2002).
11. W. R. Peltier, *Quat. Sci. Rev.* **21**, 377 (2002).
12. R. L. Edwards, *Science* **267**, 536 (1995).
13. W. R. Peltier, *Science* **267**, 536 (1995).
14. W. R. Peltier, in *Coastal Tectonics*, I. S. Stewart, C. Vita-Finzi, Eds. (Geological Society Special Publication, London, 1998), no. 146, pp. 1–30.
15. A. M. Dziewonski, D. L. Anderson, *Phys. Earth Planet. Inter.* **25**, 297 (1981).
16. Two preliminary modifications were made to the ICE-3G deglaciation model (*17*): The deglaciation chronology was revised to be consistent with the ^{14}C calibration results of Bard *et al.* (*3*) and a glaciation phase was included by reversing the deglaciation history and extending the duration of the time increments to create a glaciation period of ~100 kyr. However, further modification to this ice history was required to fit the Barbados record. In particular, the ICE-3G model underpredicts the sea-level rise at Barbados by ~15 m (*10*) and does not include a rapid rise in sea level at the time of mwp-IA. We altered the North American component of the model to address these limitations. The volume of the North American ice complex was increased by ~30% (the precise value was a function of the adopted lower mantle viscosity) in accord with recent glaciological (*38*) and geodetic (*39*) constraints and a large reduction in volume was imposed at the time of mwp-IA. The duration of the ice model time increments was reduced to 0.5 cal kyr between 15 and 13 cal kyr BP to better capture this rapid event. In creating the predictions shown in Fig. 1, we made no attempt to model the mwp-IB event at ~11 cal kyr BP (*2*).
17. A. M. Tushingham, W. R. Peltier, *J. Geophys. Res.* **96**, 4497 (1991).
18. Specifically, the revised model included 26 m from North American ice, 2 m from other northern hemisphere sources, and no contribution from Antarctica.
19. W. R. Peltier, *Science* **265**, 195 (1994).
20. W. R. Peltier, *Annu. Rev. Earth Planet. Sci.* **32**, 111 (2004).
21. G. A. Milne, J. X. Mitrovica, J. L. Davis, *Geophys. J. Int.* **139**, 464 (1999).
22. J. X. Mitrovica, G. A. Milne, *Geophys. J. Int.* **154**, 253 (2003).
23. J. X. Mitrovica, *Quat. Sci. Rev.* **22**, 127 (2003).
24. K. Lambeck, T. Purcell, P. Johnston, M. Nakada, Y. Yokoyama, *Quat. Sci. Rev.* **22**, 309 (2003).
25. W. R. Peltier, *Rev. Geophys.* **36**, 603 (1998).
26. J. X. Mitrovica, A. M. Forte, *J. Geophys. Res.* **102**, 2751 (1997).
27. K. Lambeck, C. Smither, M. Ekman, *Geophys. J. Int.* **135**, 375 (1998).
28. G. Kaufmann, K. Lambeck, *J. Geophys. Res.* **107**, 2280 (2002).
29. Lambeck *et al.* (*9*) did not include an mwp-IA event in their models; although they reported systematic discrepancies during the Lateglacial period, these do not appear to be as large as those reported in studies that include the major meltwater pulse.
30. P. U. Clark, J. X. Mitrovica, G. A. Milne, M. E. Tamisiea, *Science* **295**, 2438 (2002).
31. In addition to scenarios in which the entire Antarctic ice complex, or either the east and west portions, served a dominant source for mwp-IA, Clark *et al.* (*30*) found that the relative size of the sea-level jump across mwp-IA at Barbados and Sunda Shelf was consistent with the following freshwater sources: the Barents Sea plus Fennoscandian ice complexes, and melting distributed over all ice sheets in the ICE-3G deglaciation model (*17*) (All–ICE-3G), with a weighting given by the excess volume of the various complexes at the onset of mwp-IA. A scenario in which meltwater was distributed across the northern hemisphere only (North–ICE-3G) was also considered, but it performed less well than the above scenarios.
32. A. J. Weaver, O. A. Saenko, P. U. Clark, J. X. Mitrovica, *Science* **299**, 1709 (2003).
33. S. L. Kanfoush *et al.*, *Science* **288**, 1815 (2000).
34. G. H. Denton, T. J. Hughes, *Quat. Sci. Rev.* **21**, 193 (2002).
35. P. Huybrechts, *Quat. Sci. Rev.* **21**, 203 (2002).
36. W. E. Farrell, J. A. Clark, *Geophys. J. R. Astr. Soc.* **46**, 647 (1976).
37. I. Shennan, *J. Quat. Sci.* **14**, 715 (1999).
38. S. J. Marshall, T. S. James, G. K. C. Clarke, *Quat. Sci. Rev.* **21**, 175 (2002).
39. W. R. Peltier, *J. Quat. Sci.* **17**, 491 (2002).
40. Each index point based on fossil coral samples (Barbados, Huon, and Tahiti) is plotted such that it lies at the mean depth of the habitation range of the associated coral species. The error bar reflects the range of this habitation depth. The error bars at Huon, with the exception of the most recently acquired data (*7*), have been increased by ±1.5 m to account for the uncertainty in the tectonic correction for this region (*9*).
41. U. Radtke, R. Grün, H. P. Schwartz, *Quat. Res.* **29**, 197 (1988).
42. J. Chappell *et al.*, *Earth Planet. Sci. Lett.* **141**, 227 (1996).
43. The most recently published data from the Huon Peninsula were corrected using the rates provided by (*7*).

44. This research was supported by the Natural Environment Research Council of the UK (S.E.B.); the Natural Sciences and Engineering Research Council of Canada, the Canadian Institute for Advanced Research, and the Miller Institute for Basic Research in Science (J.X.M.); and the NSF Earth System History program (P.U.C.).

Supporting Online Material

www.sciencemag.org/cgi/content/full/1111575/DC1
Figs. S1 to S3
References and Notes

28 February 2005; accepted 16 June 2005
Published online 23 June 2005;
10.1126/science.1111575
Include this information when citing this paper.